

# Temperature profiles and thermal losses in 150 W high-intensity discharge lamps

J J Curry<sup>1</sup>, Craig J Sansonetti<sup>1</sup> and J Wang<sup>2</sup>

<sup>1</sup> National Institute of Standards and Technology, Gaithersburg, MD 20899-8422, USA

<sup>2</sup> Advanced Photon Source, Argonne National Laboratory, Argonne, IL 60439, USA

E-mail: jjcurry@nist.gov

Received 14 January 2005

Published 19 August 2005

Online at [stacks.iop.org/JPhysD/38/3086](http://stacks.iop.org/JPhysD/38/3086)

## Abstract

A series of 150 W quartz metal-halide test lamps containing four different chemistries has been studied with optical emission spectroscopy and x-ray absorption imaging. The four chemistries are pure Hg, Hg–HgI<sub>2</sub>, Hg–NaI and Hg–NaI–DyI<sub>3</sub>. Core temperatures and comprehensive distributions of Hg vapour densities were measured and combined to obtain comprehensive gas temperature distributions. The concentrations of additives in these specially designed test lamps were found to be much smaller than is typical for a commercial metal-halide lamp. As a consequence, the core temperatures in all lamps are largely characteristic of a pure Hg discharge. The gas temperature distributions have been used to determine power losses resulting from thermal conduction through the Hg vapour. The fraction of total input power dissipated thermally was found to be  $0.49 \pm 0.01$  in pure Hg, similar to published measurements for such lamps. In the Hg–NaI and Hg–NaI–DyI<sub>3</sub> lamps, thermal losses are  $0.41 \pm 0.01$  and  $0.42 \pm 0.01$ , respectively. The Hg–HgI<sub>2</sub> lamp has thermal losses of  $0.29 \pm 0.03$ .

## 1. Introduction

The ALITE II research consortium, organized by the Electric Power Research Institute, has conducted a multi-laboratory programme to study near-infrared (near-IR) losses in metal-halide high-intensity discharge lamps. In this context, near-IR refers to the spectral range between the red end of the visible (700 nm) and the transmission limit of the arc tube (about 3  $\mu\text{m}$  for fused silica and about 5  $\mu\text{m}$  for poly-crystalline alumina). Losses at wavelengths longer than this are almost entirely in the form of blackbody radiation from the arc tube and are, therefore, determined by the arc tube surface temperature.

Published measurements of near-IR losses in 400 W metal-halide lamps range from more than 25% of input power to less than 10% [1–3]. It is not clear whether this wide range of values is primarily the result of the different chemistries or of measurement errors. No results have been published for lower wattage lamps. If losses are as large as 25%, near-IR radiation constitutes a substantial loss mechanism, which, if reduced, could improve the overall luminous efficacy of metal-halide lamps.

One aspect of the ALITE II programme is the examination of the role of molecules in the absorption and emission

of near-IR radiation. Because the density and variety of molecules usually increases in moving from the core of the discharge to the wall, the determination of temperatures and densities in the mantle is of particular interest. Optical techniques are able to determine temperatures in the core [4], while x-ray techniques can be used to extend the temperature determination all the way to the discharge wall [5, 6].

A series of 150 W test lamps was fabricated by Philips Research Laboratories<sup>1</sup> in Aachen, Germany, for the purpose of studying near-IR losses in high-intensity discharges with a range of additive chemistries. The series of lamps consists of four different types, distinguished only by the number of different additive components. The simplest type contains only Hg, with complexity progressing through types containing Hg–HgI<sub>2</sub> and Hg–NaI, to the most complex type containing a four element mixture of Hg–NaI–DyI<sub>3</sub>. Identical sets of lamps were distributed to both the National Institute of Standards and Technology (NIST) and the University of Wisconsin [7] for the purpose of making complementary measurements.

<sup>1</sup> Identification of commercial names in this paper is done solely for the purpose of clarity. Such identification implies neither recommendation nor endorsement by the National Institute of Standards and Technology.

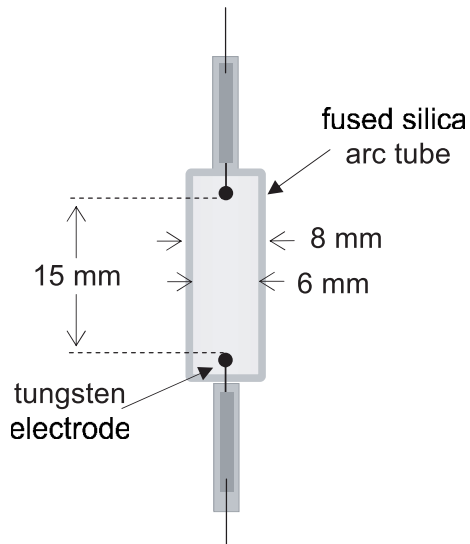


Figure 1. Geometry of the test lamps.

The work at NIST consisted of the measurement of core temperatures using optical emission spectroscopy of self-reversed lines, Hg density distributions using x-ray absorption imaging, and elemental density distributions of Hg, Dy and I using x-ray induced fluorescence. These observations indicate that the concentration of additives in the vapour phase of the test lamps is less than that required for a full transition from a pure Hg discharge to a metal-halide arc. Although this makes the test lamps not fully representative of normally-dosed metal-halide lamps, particularly with regard to the core temperature, the data do provide an opportunity to observe additive behaviour.

Here, we present results of optical emission spectroscopy and x-ray absorption measurements. The combination of core temperatures and Hg densities is sufficient to obtain complete temperature distributions in each type of lamp [8]. From these, we derived the lamp operating pressures and thermal power losses as a percentage of input power. Measurement of Hg, Dy and I densities with x-ray induced fluorescence and the corresponding distributions of molecular species inferred from a chemical equilibrium will be presented in a subsequent publication.

## 2. Lamps

The lamps examined in this study all have the same nominal geometry (figure 1) and were operated under the same conditions. They differ only in the chemical mixtures they contain. The fused silica arc tube of each lamp has an inner diameter of 6.0 mm and an outer diameter of 8.0 mm. The tungsten electrodes are separated by approximately 15 mm. These lamps do not have a jacket surrounding the arc tube, but were operated inside a stainless steel cell that was continually flushed with dry  $N_2$  to prevent oxidation of the lamp leads. This cell was equipped with x-ray windows of Al foil/polyimide or an optical window of fused silica according to the measurement being made. The lamps were burned in the vertical orientation with the shorter electrode at the bottom.

The lamps were driven by an electronic ballast at a frequency of 90 Hz. Lamp voltage and current waveforms were measured periodically during the experiments, but it was later determined that the current measurements were not reliable. Direct measurements of lamp power during the measurements described in this paper were, therefore, not obtained. Later measurements of lamp power showed the ballast to be operating at 134 W rather than the nominal 148 W. In the remainder of this paper, we assume the input power to the lamps to have been 134 W.

The set of lamps consists of four types representing a range of chemistries from simple to complex. All lamps contain 3.5 mg of Hg and 5 kPa (40 Torr) of Ar. Type 1 contains no additives, type 2 contains 0.1 mg of  $HgI_2$ , type 3 contains 0.15 mg of NaI and type 4 contains 0.18 mg of NaI and 0.29 mg of  $DyI_3$ .

## 3. Core temperatures by analysis of self-reversed line emission

We measured core temperatures in the vertical mid-planes of five of the lamps, including all four types, by analysing the magnitude and shape of self-reversed optical emission lines. This technique was first used by Cowan and Dieke [9] and by Bartels [10, 11] to extract point temperature measurements from line of sight observations. In observing a self-reversed line emitted from an arc, the intensity at the point of self-reversal is approximately equal to the intensity of a blackbody at the temperature of the hottest point along the line of sight. This is based on the assumption that the populations of the two atomic levels connected by the observed transition are in thermal equilibrium. The technique has been further developed by Karabourniotis [4] who pointed out that, in the presence of non-equilibrium excitation of atomic levels, the relative population distribution between the  $6^3P_0$  and  $6^3P_2$  metastable levels of Hg should give the best indication of the true electron temperature. These levels can be studied via the 4047 Å and 5461 Å lines, which connect these two metastable levels to the higher-lying  $7^3S_1$  level (figure 2). An effective emissivity that accounts for the finite opacity of the arc is determined by making a series of observations at several different displacements from the centre of the arc [4].

We used a 2 m Fourier transform spectrometer (FTS) to observe emission over the spectral range from approximately 3000 Å to more than 10 000 Å. Each lamp was imaged with a magnification of 1.3 onto the 0.62 mm circular entrance aperture of the FTS using a concave mirror (figure 3). The solid angle of observation is constrained by the  $f/35$  optics of the spectrometer. The projection of the entrance aperture back onto the arc lamp defines a viewing cone with a minimum diameter of 0.48 mm. If the entrance aperture is not focused accurately in the arc, the spatial resolution may be larger, but not smaller, than the minimum diameter. This gives a spatial resolution for the optical observations of 0.48 mm with an uncertainty of +0.06 mm. By moving the lamps horizontally on a translation stage, we observed spectra along nine lines of sight through the mid-plane of each arc over a range of displacements  $x$  from the centre (see figure 4). Observations were made at 0.50 mm intervals.

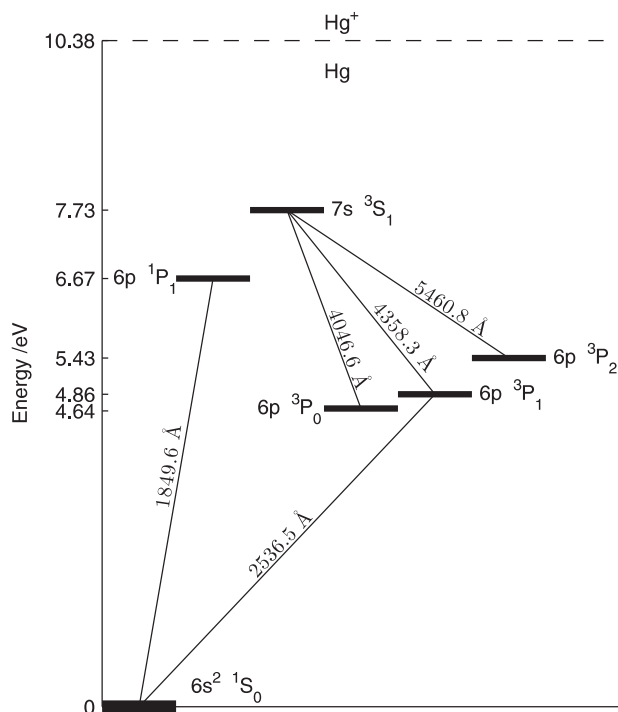


**Figure 2.** Some transitions and energy levels of Hg. Transition wavelengths are air values except for 1849.5 Å, which is the vacuum value.

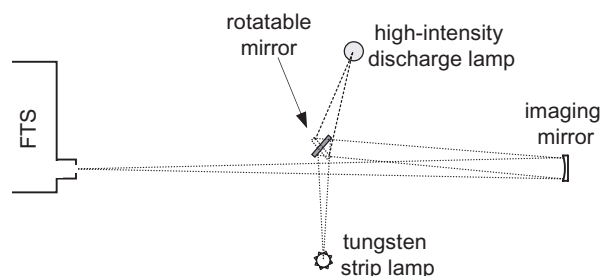


**Figure 3.** Schematic diagram of the optical set-up used to calibrate emission spectra observed with a FTS by comparison to a radiometric standard tungsten strip lamp.

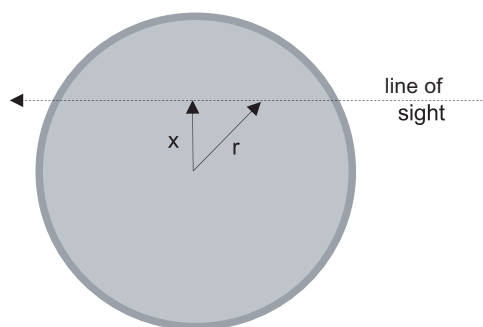


**Figure 4.** Geometry for line-of-sight observations of both optical emission and x-ray absorption.

A radiometrically calibrated tungsten strip lamp was observed before and after the full set of spatially resolved spectra for each arc lamp. The strip lamp was imaged onto the entrance aperture by a simple rotation of the flat mirror in figure 3. Linear combinations of the initial and final calibration

spectra were used to derive an instrument response function for each arc lamp spectrum. These response functions were used to calibrate intensities from the arc lamps on an absolute scale. However, only relative intensities are required for the measurements reported here.

An advantage of the FTS for this application is its simultaneous acquisition of data at all wavelengths. This eliminates errors in comparing the intensities of widely separated spectral features that can arise due to source drifts during data acquisition and calibration. The FTS also has the advantages of high resolving power and strong immunity from spurious background contributions due to scattered light. Data acquired by the FTS cannot be time-resolved with respect to the phase of the lamp drive frequency. This is not a serious limitation in the present case because the lamps were driven by an electronic ballast with square wave excitation producing a nearly dc light output.

One drawback of spectra recorded with the FTS is that the noise in the spectrum is determined principally by the total light detected and is distributed uniformly over the entire spectral range. This is particularly disadvantageous in using the tungsten strip lamp as a radiometric standard. The spectrum of the tungsten lamp is dominated by strong infrared emission, resulting in low signal-to-noise ratio for the much weaker spectrum in the blue. Despite the fact that the spectra were strongly smoothed to suppress this random noise, comparison of the initial and final calibration spectra indicate that the relative calibration uncertainty between the Hg lines at 4047 and 5461 Å is 3% for lamps 4259 (Hg), 3234 (Hg + NaI), 4278 (Hg + NaI) and 4251 (Hg + NaI + DyI<sub>3</sub>) and is 10% for lamp 4226 (Hg + HgI<sub>2</sub>). These are systematic uncertainties since the spectra from each lamp were calibrated as a set using the same initial and final tungsten lamp spectra. The impact of strong infrared emission on the calibration spectra was not fully appreciated until after the measurements were made. In future work, these calibration uncertainties can be reduced by using optical filters to reject infrared light.

The Hg 4047 Å and 5461 Å lines are strongly self-reversed in pure Hg arcs and are also self-reversed in the lamps with more complex chemistries due to the relatively small additive concentrations. Figure 5 shows a spectrum from one of the Hg–NaI–DyI<sub>3</sub> lamps, with the 4047 Å and 5461 Å lines expanded in insets. Despite the presence of additives, the principal emission lines of Hg dominate the spectrum. The integrated intensity of the Hg 5461 Å line is approximately four times larger than the integrated intensity of the self-reversed Na D-lines at 5890 Å and 5896 Å. These relative intensities are approximately the same in the Hg–NaI lamps. The Hg–HgI<sub>2</sub> lamp spectra show little sign of radiation from I<sub>2</sub> or I in the spectral range of observation. The pure Hg lamp spectra contain many lines of W that undoubtedly originate from the electrodes. These lines are strongly suppressed in lamps containing I and are absent in lamps containing Na.

#### 4. Mercury distributions by x-ray absorption imaging

We measured comprehensive Hg density distributions in all eight test lamps using x-ray absorption imaging with synchrotron radiation from the Advanced Photon

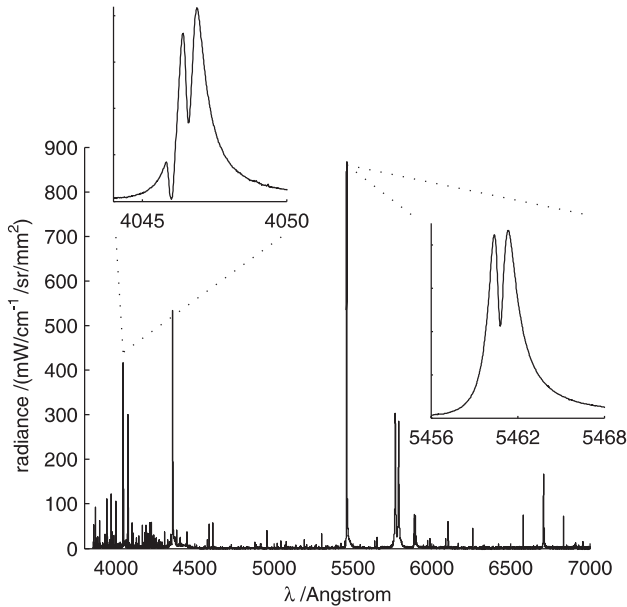


**Figure 5.** Optical emission spectrum from the centre of a Hg–NaI–DyI<sub>3</sub> lamp, with the 4047 Å and 5461 Å lines highlighted. The Dy I 4046 Å resonance line is seen in absorption.

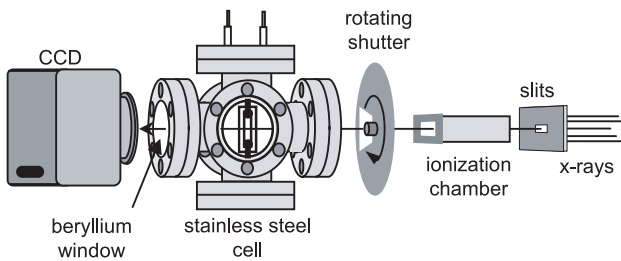


**Figure 6.** X-ray absorption imaging using synchrotron radiation and a CCD detector.

Source (APS). This technique has been described previously [12], so only a brief summary is given here. The Sector 1 Bending Magnet Beam Line at the APS delivered a collimated beam of monochromatic x-rays to the experimental layout shown in figure 6. Beam line optics and attributes are described by Lang *et al* [13]. The beam line optics were adjusted to produce a beam with maximum area and minimum spatial structure [14]. A pair of  $x$ - $y$  slits was used to define a beam approximately 15 mm wide by 6 mm high at the lamp. The limited beam size did not allow us to examine the entire vertical extent of a lamp in a single image, but did allow us to see the entire width at a given height. Five vertically displaced images were sufficient to observe the entire lamp.

The transmission of 19 keV x-rays through the Hg vapour in each arc lamp was measured with an x-ray sensitive charge-coupled device (CCD) detector. The beam-integrated incident flux was continuously monitored with a gas-filled ionization chamber to ensure accurate determination of the absolute transmission. The CCD detector contains an integrated phosphor layer that converts x-ray photons into visible photons. The phosphor is coated onto one end of a fibre-optic bundle, which is bonded directly to the 25.9 mm  $\times$  27.5 mm CCD chip. The CCD pixel size is 22.5  $\mu$ m  $\times$  22.5  $\mu$ m, but the measured linear spatial resolution of the entire system is approximately 60  $\mu$ m full-width at half-maximum.

In previous work [12], we used the intensifier of an intensified CCD detector to synchronously gate the acquisition of data. This allowed us to obtain time-resolved measurements in different phases of the alternating current cycle and during the cool-down period [6, 15]. In the present case, we are interested in time-averaged measurements and the use of an *un*-intensified CCD eliminates noise generated by the intensifier. It is still necessary, however, to accurately gate the flux of photons onto the CCD in order to obtain a controlled integration time and to allow time for the CCD to be read without additional exposure. A typical exposure time is of the order of 100 ms, allowing us to use a mechanical shutter to block the x-ray beam. A tungsten disc with a wedge-shaped hole was mounted on a stepper motor for this purpose. The stepper motor turned the aperture through the x-ray beam with a velocity sufficient to produce the desired exposure of the CCD. While the CCD was being read, the motor was idle with the beam blocked. We verified that this method, when used with a typical exposure time of 15 alternating current cycles, gave CCD exposures reproducible to better than 1%, the limit of photon statistics during the test.

Column densities of Hg observed as a function of distance,  $x$ , from the arc axis were Abel inverted to obtain the local Hg density as a function of radial position,  $r$  (see figure 4). The Abel inversion was implemented by fitting the observed column densities with special polynomial functions,  $G_n(x)$ , whose Abel inversions are analytic and proportional to  $r^n$  [12]. Terms up to  $n = 16$  were utilized, resulting in a spatial resolution of approximately 300  $\mu$ m. This is much finer spatial resolution than was achieved in earlier work [6, 12] and allows us to more fully resolve the steep gradients in density and temperature near the wall. (The measured column densities are also smaller than in previous work as a result of the smaller lamp size.) The inclusion of higher-order terms also has the undesired effect of propagating some of the measurement noise through the Abel inversion. This noise tends to accumulate on the axis, producing unphysical ripples in the density. We have eliminated these ripples by re-fitting the middle half of each radial profile with a polynomial containing terms only up to  $n = 4$ , reducing the spatial resolution in the core to approximately 750  $\mu$ m. This procedure does not remove any significant information from the data.

An example of a density profile from the mid-plane of one of the test lamps is shown in figure 7. This profile is spatially averaged over 1 mm parallel to the lamp axis. In other words, the mean density is derived from 44 adjacent rows of CCD pixels. The spatial averaging reduces noise without loss of significant information as axial gradients are small in this region of the lamp. Results for the other seven test lamps are very similar, with agreement in the range of 5% to 10%. This level of agreement generally holds throughout the rest of the arc volume. An example of a full image of the Hg density distribution in one of these lamps can be seen in [16].

Random errors in the mean density as a function of  $r$  can be approximated as the standard deviation of the mean over the sample of 44 rows. The relative uncertainties so derived are shown as a dashed line in figure 7. The relative uncertainty has a local maximum of slightly less than 2% near the wall because absorption by the arc tube leads to a minimum in the detected x-ray flux. The uncertainty has a global maximum of slightly greater than 2% on-axis. As mentioned above,

errors tend to accumulate at  $r = 0$  because the Abel inversion determines the density at radius  $r$  from the measured line-of-sight transmissions at all  $x \geq r$ . Between the wall and the core, the random relative uncertainty is approximately 1%. The uncertainties in figure 7 are typical for averaged radial distributions in the mid-planes of all the lamps.

Systematic errors in the density measurements are limited by the nature of the measurement. Since transmission is obtained by taking the ratio of the x-ray flux through the operating lamp and the cold lamp, errors common to the measurement of flux through both the hot and cold lamp are eliminated. Systematics that are not eliminated include such things as uncertainties in the relative incident flux (estimated at less than 1%), errors in the Hg absorption cross-section (estimated at less than 1%), changes in the arc during the measurement period (unknown) and any systematic errors introduced by the inversion algorithm (unknown).

An excellent check on systematic error can be obtained by integrating the measured Hg density over the entire lamp volume and comparing the result to the known Hg dose. The results, given in table 1, agree well with the nominal dose of 3.5 mg of Hg per lamp. The average measured dose is  $3.60 \pm 0.18$  mg. As no arbitrary scaling was used to obtain

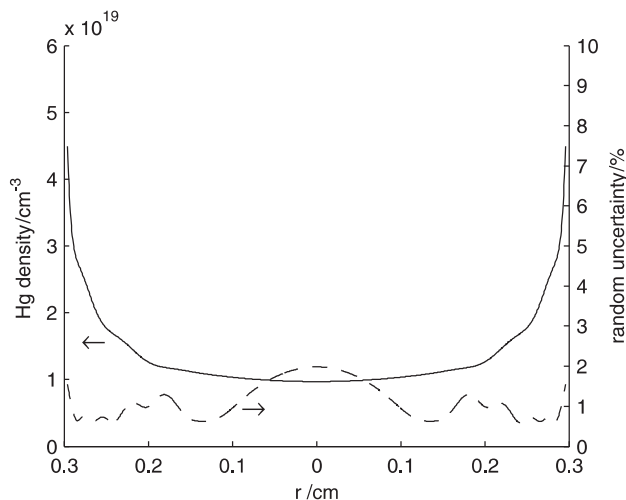


**Figure 7.** The mean of 44 adjacent radial profiles of Hg density (corresponding to 1 mm along the axis) from the mid-plane of one of the pure Hg lamps (—) and the standard deviation in the mean (---), which we take as the component of uncertainty arising from random effects.

**Table 1.** Measured parameters of interest for eight test lamps operating at 134 W.

Lamp No.	Mix	Hg (mg)	Gap (mm)	Pressure (MPa) (atm <sup>-1</sup> )	Voltage (V)	$T_{\text{peak}}$ (K)	$P_{\text{thermal}}/P_{\text{input}}$
4259	Hg	$3.78 \pm 0.08$	15.3	$0.94(9.3) \pm 0.03(0.3)$	$84 \pm 2$	$6660 \pm 140$	$0.49 \pm 0.013$
4255	Hg	$3.86 \pm 0.08$	14.3		$75 \pm 1$		
4226	Hg–HgI <sub>2</sub>	$3.46 \pm 0.07$	14.4	$0.75(7.4) \pm 0.05(0.5)$	$79 \pm 2$	$6350 \pm 440$	$0.29 \pm 0.025$
4268 <sup>a</sup>	Hg–HgI <sub>2</sub>		14.9		$86 \pm 1$		
4234	Hg–NaI	$3.58 \pm 0.07$	14.4	$0.86(8.5) \pm 0.03(0.2)$	$85.5 \pm 0.5$	$6480 \pm 140$	$0.41 \pm 0.011$
4278 <sup>a</sup>	Hg–NaI		14.6	$0.75(7.4) \pm 0.02(0.2)$	$78.5 \pm 0.5$	$6500 \pm 140$	
4251	Hg–NaI–DyI <sub>3</sub>	$3.49 \pm 0.07$	14.2	$0.85(8.4) \pm 0.02(0.2)$	$83.5 \pm 1.5$	$6410 \pm 130$	$0.42 \pm 0.011$
4285	Hg–NaI–DyI <sub>3</sub>	$3.45 \pm 0.07$	14.7		$87 \pm 1$		

<sup>a</sup> Optical emission spectra not observed for this lamp.

<sup>b</sup> At least one electrode is off-centre, leading to an asymmetric arc and much higher uncertainties in the determination of total Hg dose and thermal losses. Therefore, these numbers are not reported.

this result, it lends a high degree of confidence to the accuracy of the x-ray absorption imaging technique. We believe that overall systematic errors due to the inversion algorithm and monotonic changes in the arc during measurement are limited to no more than 5%.

Electrode gaps were also measured from the absorption images and are given in table 1.

## 5. Results and discussion

Electron temperature profiles obtained from observations of the self-reversed Hg 5461 Å and 4047 Å lines in the mid-planes of five lamps are shown in figure 8. Temperatures in the core range from approximately 6300 K to 6600 K, higher than expected for a metal-halide arc, but not unusual for a discharge dominated by Hg. It is interesting to note the close agreement between the results for the two Hg–NaI lamps. This is the only lamp type for which two samples were observed optically.

The core temperatures shown in figure 8 can be extended throughout the entire arc using the Hg density distributions obtained from x-ray absorption imaging. Treating the Hg vapour as a monatomic ideal gas, the lamp pressure is determined from

$$p_0 = n_{\text{Hg}}(r = 0, z_0)kT_{\text{gas}}(r = 0, z_0),$$

where  $k$  is Boltzmann's constant and we have assumed

$$T_e(r = 0, z_0) = T_{\text{gas}}(r = 0, z_0).$$

Pressure gradients that drive convective flow in high-intensity discharge lamps are small enough to be negligible in this context [17, 18]. Lamp pressures obtained in this way are given in table 1, and range from 0.77 MPa (7.6 atm) to 0.95 MPa (9.4 atm).

Once  $p_0$  is known,  $T_{\text{gas}}$  can be obtained for all  $r$  and  $z$ , again using the ideal gas law. Full radial profiles of the gas temperature in the mid-planes of the five lamps for which optical spectra were obtained are shown in figure 9. Each profile represents a spatial average over 1 mm parallel to the axis. These profiles are notable for their accuracy in the mantle and near the wall where optical measurements are practically impossible. This is the region where molecules are expected to play a role in the production and absorption of infrared radiation losses.

Uncertainties in the arc temperature increase near the wall because of the increase in uncertainty for the Hg density

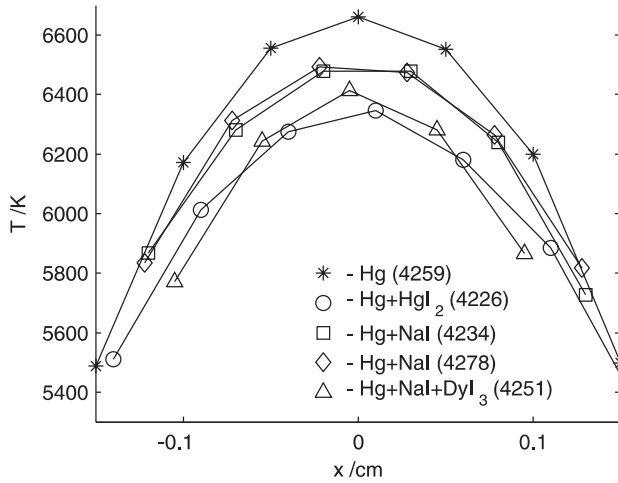


**Figure 8.** Electron temperatures in five of the eight test lamps, obtained from observation of self-reversed optical emission lines. Random uncertainties are too small to be seen on this scale. Systematic uncertainties are  $\pm 7\%$  for the Hg–HgI<sub>2</sub> lamp and  $\pm 2\%$  for the other lamps.

(see figure 7). This results from the reduced signal obtained in the x-ray absorption imaging in this region and from the large gradients in temperature and density. Nevertheless, it is interesting to note that the measurements give temperatures in the range of 1200–1650 K in this region. A typical operating wall temperature in the mid-plane of a quartz lamp is approximately 1200 K. Recognizing that the x-ray absorption imaging results cannot be extended to closer than 50–100  $\mu\text{m}$  from the wall, and that the temperature is rapidly decreasing in this region, these measured temperatures are reasonable.

Complete temperature distributions make it possible to determine absolute thermal power losses

$$P_{\text{th}} = \oint \kappa(T) \nabla T_{\text{gas}}(r, z) \cdot dS,$$

where  $\kappa$  is the thermal conductivity of pure Hg and  $S$  is a closed surface containing the arc core. This integral increases monotonically as the surface of integration expands outwards, indicating the deposition of radiation in the cooler mantle layers. The integral reaches a maximum, as a result of the finite spatial resolution of the density measurement, when the

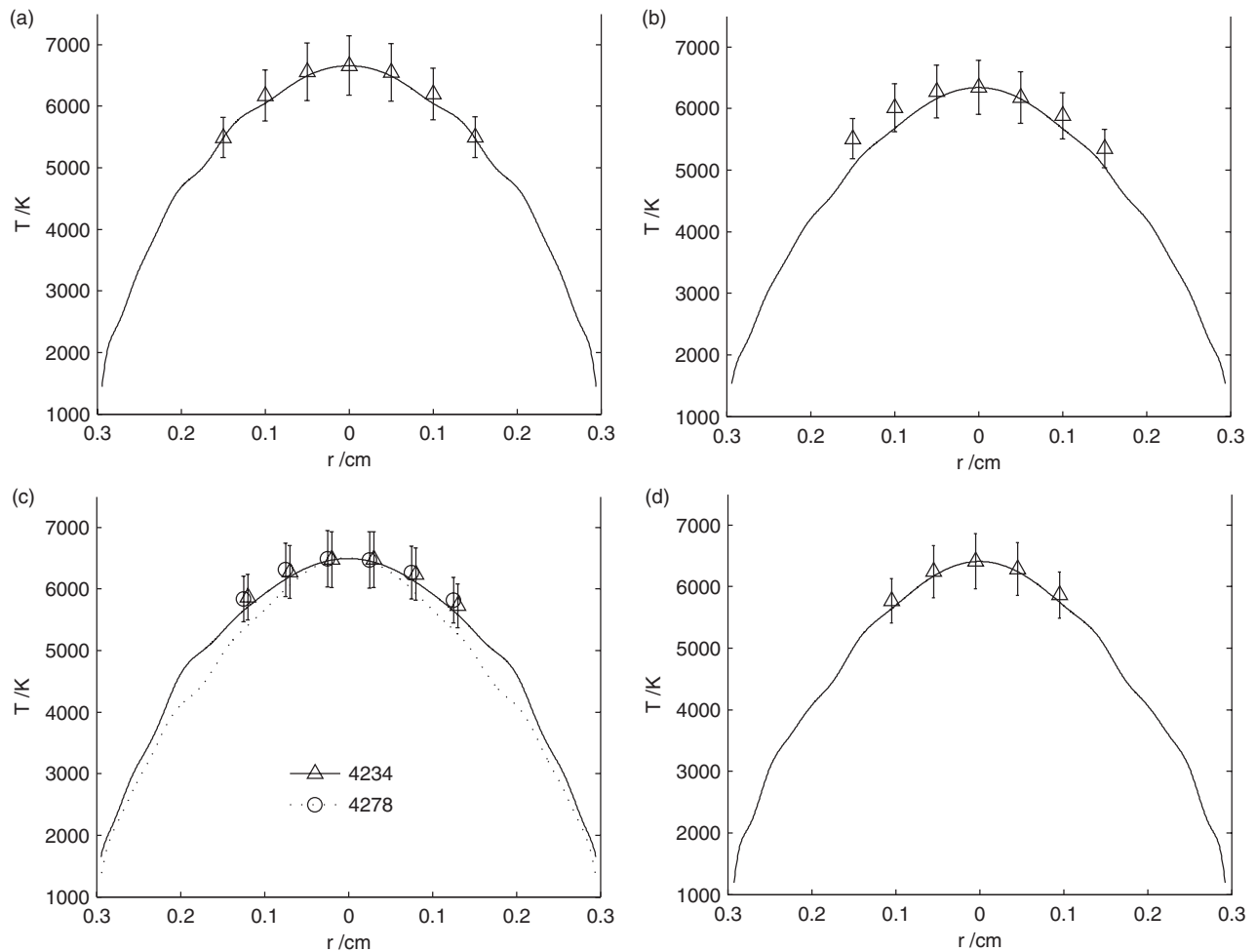


**Figure 9.** Radial profiles of temperature in the mid-planes of high-intensity discharge lamps with four chemistries. The data points are derived from optical emission measurements. The curves represent the temperature profiles derived using Hg density distributions measured by x-ray absorption imaging. (a) Lamp No. 4259, pure Hg. (b) Lamp No. 4226, Hg–HgI<sub>2</sub>. (c) Lamp Nos. 4234 and 4278, Hg–NaI. (d) Lamp No. 4251, Hg–NaI–DyI<sub>3</sub>.

surface is within a few pixels of the arc tube. In this region, only kinetic contributions to the thermal conductivity need be considered, and the data of Svehla [19] are approximated by the analytic formula

$$\kappa = 6.3 \times 10^5 T^{0.8} \text{ W K}^{-1} \text{ cm}^{-1}.$$

With the surface chosen to maximize the integrand, thermal losses, not including power lost through the electrodes, are reported in table 1. The fraction of total input power lost to thermal dissipation in the pure Hg lamp is  $0.49 \pm 0.01$ , slightly higher than published results for Hg lamps. Jack and Koedam [1] found thermal losses of 45% for a 400 W Hg lamp, with few details of the geometry or pressure given. Lister and Waymouth [20] give thermal losses of 38%, also for 400 W Hg lamps. No uncertainties were given by either of these sources. The Hg–NaI and Hg–NaI–DyI<sub>3</sub> lamps have somewhat lower thermal loss fractions of  $0.41 \pm 0.01$  and  $0.42 \pm 0.01$ , respectively. Lower losses are expected for lamps containing additives because of increased radiation, but the reduction is modest because of relatively low additive densities, as discussed earlier. The thermal loss fraction for the Hg–HgI<sub>2</sub> lamp is significantly lower at  $0.29 \pm 0.03$ . This may be the result of increased radiative losses by molecular or atomic iodine, although we see no evidence of this in the spectral range of 3000–10 000 Å. The uncertainties given for thermal losses, as well as for other measurements presented in this paper, do not reflect uncertainties in the reproducibility of arc conditions or sample-to-sample variations. The uncertainties for the percentages of power in thermal losses do not reflect uncertainty in the input power to the lamps (see section 2).

The high core temperatures as well as the similarities in the temperatures and densities of the different lamp types reinforces our conclusion from the optical spectra that the additives in these test lamps are not sufficiently abundant to produce substantial changes in arc properties.

## 6. Summary

Core temperatures in a series of 150 W high-intensity discharge lamps with increasingly complex additive doses have been obtained by analysis of self-reversed optical emission lines. Comprehensive Hg density distributions have been obtained by x-ray absorption imaging, yielding volume-integrated Hg densities in excellent agreement with the nominal doses. The core temperatures and Hg density distributions were combined to give lamp pressures and complete temperature distributions. These temperature

distributions are notable for their accuracy in the mantle. All the lamps are seen to be similar to pure Hg lamps as a result of low additive densities. Core temperatures range from 6300 K to 6600 K with pressures ranging from 0.75 MPa (7.4 atm) to 0.94 MPa (9.3 atm). Thermal losses determined from temperature distributions are 49% in pure Hg, 42% in Hg–NaI–DyI<sub>3</sub>, 41% in Hg–NaI, and 29% in Hg–HgI<sub>2</sub>. Measurements of the elemental densities of Hg, Dy and I in the same lamps using x-ray induced fluorescence will be described in a subsequent publication.

## Acknowledgments

Funding for the ALITE II lighting research consortium is provided by the Electric Power Research Institute and Philips Lighting. Use of the Advanced Photon Source was supported by the US Department of Energy, Basic Energy Sciences, under contract No. W-31-109-Eng-38.

## References

- [1] Jack A G and Koedam M 1974 *J. Illum. Eng. Soc.* **3** 323
- [2] Keefe W M 1975 *J. Illum. Eng. Society* **4** 260
- [3] Smith D J, Bonvallet G A and Lawler J E 2003 *J. Phys. D: Appl. Phys.* **36** 1519
- [4] Karabourniotis D 2001 *J. Appl. Phys.* **90** 1090
- [5] Curry J J, Adler H G, Shastri S D and Lee W K 2003 *J. Appl. Phys.* **93** 2359
- [6] Curry J J, Adler H G, MacPhee A, Narayanan S and Wang J 2004 *Plasma Sources Sci. Technol.* **13** 403
- [7] Lawler J E, Koerber A and Weichmann U 2005 *J. Phys. D: Appl. Phys.* **38** 3071 (this issue)
- [8] Curry J J, Adler H G, Lee W K and Shastri S D 2003 *J. Phys. D: Appl. Phys.* **36** 1529
- [9] Cowan R D and Dieke G H 1948 *Rev. Mod. Phys.* **20** 418
- [10] Bartels H 1950 *Z. Phys.* **127** 243
- [11] Bartels H 1950 *Z. Phys.* **128** 546
- [12] Curry J J, Sakai M and Lawler J E 1998 *J. Appl. Phys.* **84** 3066
- [13] Lang J C, Srajer G, Wang J and Lee P L 1999 *Rev. Sci. Instrum.* **70** 4457
- [14] Assoufid L, Lang J, Wang J and Srajer G 1998 *Proc. SPIE* **3447** 109
- [15] Curry J J, Sansonetti C J, Hechtfisher U and Adler H G 2002 *Bull. Am. Phys. Soc.* **47** 38
- [16] Curry J J and Sansonetti C J 2005 *IEEE Trans. Plasma Sci.* at press
- [17] Zollweg R J 1978 *J. Appl. Phys.* **49** 1077
- [18] Lowke J J 1979 *J. Appl. Phys.* **50** 147
- [19] Svehla R A 1962 *Techn. Rep.* R-132 NASA
- [20] Lister G G and Waymouth J F 2002 *Encyclopedia of Physical Science and Technology* 3rd edn, vol 8 (New York: Academic) p 557